Journal of

Applied and Computational Mechanics

Shahid Chamran
University of Ahvaz

Research Paper

A Meshless Method based on Moving Kriging Interpolation for the Numerical Solution of the Transient Flow of Magnetohydrodynamic Fractional Maxwell Fluid Equation

Ali Habibirad[1], Esmail Hesameddini[2], Younes Shekari[3], Mohammad Hossein Heydari[2], Omid Baghani[1]

[1] Department of Mathematics and Computer Sciences, Hakim Sabzevari University, Sabzevar, Iran,
Email: a.habibirad@sutech.ac.ir (A.H.); omid.baghani@gmail.com (O.B.); O.baghani@hsu.ac.ir (O.B.)

[2] Department of Mathematics, Shiraz University of Technology, Shiraz, Iran, Email: hesameddini@sutech.ac.ir (E.H.); heydari@sutech.ac.ir (M.H.H.)

[3] Department of Mechanical Engineering, Yasouj University, Yasouj, Iran, Email: Shekari@yu.ac.ir

Abstract. Maxwell model is one of the most outstanding and widely used models for the description of viscoelastic materials. In this study, we use an efficient meshfree technique based on the Moving Kriging (MK) interpolation for the numerical solution of Magnetohydrodynamic (MHD) flow of fractional Maxwell fluid. In this scheme to discretize this equation in time and space variables, we use the finite difference method and MK interpolation shape functions, respectively. Also, we calculate the local weak form for every node instead of the computation of the global weak form for the global domain. So, we reduce such problems to a system of algebraic equations. To indicate the efficiency of the present scheme, four examples are discussed in various types of domains and with uniform and nonuniform nodal distribution in 2D cases. Also, to show the validity of the method in this example, a comparison with a valid method has been made. Moreover, in the last example, the accuracy of our scheme in the 3D case is illustrated for the fractional telegraph equation.

1. Introduction

In recent times, fractional differential equations (FDEs) and their applications have been fundamental and popular. The origin of this branch of differential equations was first proposed in a letter from Leibniz to L'Hospital in 1695 [1]. FDEs and fractional calculus have many applications in various branches of engineering and sciences such as chemistry, physics, fluid mechanics, viscoelasticity, finance, signal processing, biology, and so on [2-5]. Difficulty to find an analytical solution of FDEs motivated researchers to solve these equations numerically. Many numerical schemes have been applied and developed for the numerical solution of PDEs, such as finite element methods [6-10], homotopy analysis schemes [11-12] variational iteration methods [13-15], and collocation schemes see [16-21]. Some of the mentioned references are based on mesh-dependent schemes. Also, Grid generation of complex geometries is itself a difficult task.

Therefore, the meshfree technique has become a broad issue in the research community. Dehghan et al. [22] applied a meshfree technique based on the radial basis function (RBF) and the Kansa method for the numerical solution of the time-fractional nonlinear Kline-Gordon and Sine-Gordon equations. Salehi [23] proposed a meshfree collocation technique to solve multi-term time-fractional diffusion wave equation. Shivanian applied an applicable meshless scheme named as spectral meshfree radial point interpolation (SMRPI) technique [24] for solving the two-dimensional diffusion equation with an integral condition.

Shokri and Habibirad [25] applied the MLPG method for the nonlinear Kline-Gorden equation. The main benefit of the MLPG method is to transform a global approximation into a system of algebraic equations for the numerical solution of a problem. Also, it uses a local weak form in each sub-domain instead of a global weak form. There are six different types of MLPG techniques created by changing the test function which are named as MLPG1, MLPG2, … and MLPG6. Habibirad et al. [26] presented an efficient combination of the MLPG5 and time-splitting methods for the numerical solution of the nonlinear Schrodinger equation in two and three dimensions. Among these six methods, the MLPG2 is a collocation-type method.

Habibirad et al. [27] proposed the MLPG2 method for solving the two-dimensional variable-order time-fractional mobile/immobile advection-diffusion model with Dirichlet boundary conditions. In all versions of MLPG, the authors used moving

least square (MLS). The MLS shape functions don't have the Kronecker delta attribute. So, imposing the essential boundary condition is difficult. Here, to eliminate this deficiency, we use Moving Kriging (MK) interpolation to form the MLPG shape functions. Many researchers used MK instead of MLS in the MLPG method. For example, we refer the readers to [25-27] and references therein. In this paper, we apply the MLPG approach for the numerical solution of the unsteady 2D flow of magnetohydrodynamic (MHD) fractional Maxwell fluid.

Viscoelastic fluids show both the elastic behavior of solids and viscose characteristics of liquids simultaneously. Some materials such as soap solutions, paints, polymer melts, etc., show viscoelastic behavior. These fluids are used in several industrial and life science applications, including oil exploitation [28, 29], wire coating [30], blood flow in human arteries [31], and many others. Therefore, the study of viscoelastic fluids and their mathematical modeling has significant importance in the optimum design of industrial processes and facilities.

There are several models for the mathematical modeling of such fluids, including Maxwell, Voigt, Jeffreys, Oldroyd, KBZ, etc. [32] Maxwell model is one of the most outstanding and widely used models for describing viscoelastic materials [33, 34], among others. However, one of the weaknesses of this model arises when it is used for modeling simple shear flows of natural fluids [39]. In this situation, the model cannot predict the relationship between shear stress and shear rate accurately. Therefore, some modifications should be considered to improve its performance in describing simple shear flows.

The memory of fluids is one of the most important and most ignored characteristics of them since this property represents the history of the fluid and affects its future behavior [36]. On the other hand, time-fractional models can save the memory of systems. Therefore, several investigators used fractional-order derivatives to mathematical modeling of viscoelastic fluids [37, 38]. In this way, the integer orders of conventional viscoelastic models are replaced by real orders to obtain a fractional viscoelastic model. The fractional version of the Maxwell model has an excellent description of experimental data [35]. Therefore, one may overcome the drawback mentioned above in the modeling of simple shear flows.

MHD flow arises in several applications, including the flow of saltwater, electrolytes, MHD casting of liquid metals (see Fig. 1), etc. In such flows, a magnetic field can affect the hydrodynamic and heat transfer of a flowing conductive fluid. Several scientists investigated the flow of MHD fractional viscoelastic fluids in different situations [38-44].

In this study, we consider a fully developed flow in a pipe with four- different cross-sectional area, as shown in Fig. 2. Therefore, we neglect the velocity variation in the axial direction, and then one has a 2D velocity profile that just varies in x and y directions. Hence, the governing equation for the 2D fully developed flow of MHD fractional Maxwell fluid and the associated initial and boundary conditions are as follows:

$$\begin{cases} \mathcal{D}_t^{\alpha} v(\mathbf{p},t) + \lambda_1 \mathcal{D}_t v(\mathbf{p},t) + \lambda_2 \mathcal{D}_t^{\beta} v(\mathbf{p},t) + \lambda_3 v(\mathbf{p},t) = \lambda_4 \Delta v(\mathbf{p},t) + s(\mathbf{p},t), & (\mathbf{p},t) \in \Omega \times [0,T], \\ v(\mathbf{p},0) = v_0(\mathbf{p}), \quad v_t(\mathbf{p},0) = g(\mathbf{p}), & \mathbf{p} \in \Omega, \\ v(\mathbf{p},t) = h(\mathbf{p},t), & \mathbf{p} \in \partial\Omega, \end{cases} \quad (1)$$
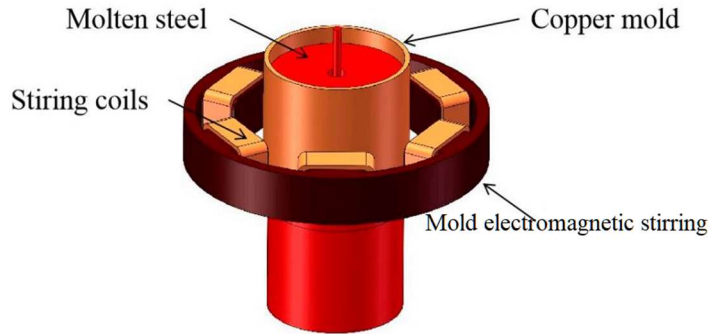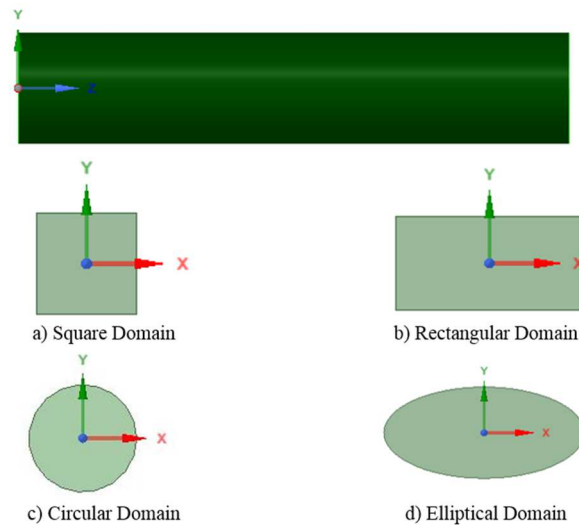

Fig. 1. MHD casting of liquid metals [52].

Fig. 2. Schematic of problem geometry and the cross-sectional area of the selected domains.

Table 1. Nomenclature section of the paper.

Parameter Notation	Parameter Definition	Unit
T	Final time	s
α	Caputo fractional derivative order	Constant number
β	Caputo fractional derivative order	Constant number
λ	Relaxation time	s
M	Pressure gradient parameter	Constant number
$\lambda_1 := \dfrac{1}{\lambda^\alpha}$	Dependent quantity	$\dfrac{1}{s}$
$\lambda_2 := M$	Pressure gradient parameter	Constant number
$\lambda_3 := \dfrac{M}{\lambda^\alpha}$	Dependent quantity	$\dfrac{1}{s}$
$\lambda_4 := \dfrac{1}{\lambda^\alpha}$	Dependent quantity	$\dfrac{1}{s}$
τ	Time step size	s

where, $1 < \alpha \leq 2, \beta = \alpha - 1$, and $\Omega \subset \mathbb{R}^2$. Also, T is the final time, and $\mathfrak{D}_t^\zeta$ is the Caputo fractional derivative operator concerning t defined as follows:

$$
\mathfrak{D}_t^\zeta v(\mathbf{p},t) = \begin{cases} \dfrac{1}{\Gamma(l-\zeta)} \displaystyle\int_0^t \dfrac{\partial^l v(\mathbf{p},r)}{\partial r^l} \dfrac{dr}{(t-r)^{\zeta-(l-1)}}, & l-1 < \zeta < l, \\ \dfrac{\partial^l v(\mathbf{p},t)}{\partial t^l}, & \zeta = l, \end{cases} \tag{2}
$$

in which l is a positive integer. In Eq. (1), Δ is the Laplacian differential operator $\Delta = \partial^2() / \partial x^2 + \partial^2() / \partial y^2$. Moreover, v_0, g, s and h are given functions. Zhang et al. [37] studied the analytical and numerical solutions for the 2D flow of MHD fractional Maxwell fluid (1) in a rectangular pipe driven by a variable pressure gradient. A list of nomenclature used throughout this paper is provided in Table 1.

This paper is constructed by the following sections: In Section 2, we give a brief review of the MK interpolation. In Section 3, we explain the time discretization and numerical performance of the MLPG technique based on MK interpolation for the MHD fractional Maxwell fluid equation. A numerical experiment is performed for the mentioned equation in Section 4. Finally, a brief conclusion is given in Section 5.

2. A Summary of Construction MK Interpolation Shape Functions

In meshless schemes, several methods are employed to build the shape functions, such as the radial basis function (RBF) technique, and moving least square (MLS) scheme [25, 26, 45]. The moving Kriging interpolation approach introduces different kinds of shape functions in meshless techniques. These shape functions have the $\delta -$ Kronecker attribute. So, the essential boundary conditions can be imposed easily. The Kriging and its derivatives are used to interpolate geostatistical data [46, 47]. Suppose the global domain $\Omega \subseteq \mathbb{R}^2$ is discretized with some of properly scattered points $\mathbf{x}_i, i = 1,2,\dots,n$ and $v(\mathbf{x})$ is a function defined in Ω. Suppose that only N points surrounding node $\mathbf{x}$ influence $v(\mathbf{x})$. The MK technique $v^h(\mathbf{x})$ is formulated as follows [46, 48]:

$$
v^h(\mathbf{x}) = \sum_{i=1}^N \phi_i(\mathbf{x}) v_i = \Phi(\mathbf{x})\mathbf{v}, \quad \mathbf{x} \in \Omega_x, \tag{3}
$$

in which the shape functions ϕ_i is:

$$
\phi_i(x) = \sum_{j=1}^m p_i(x)\mathcal{A}_{ji} + \sum_{k=1}^N r_k(x)\mathcal{B}_{ki}, \tag{4}
$$

where $\mathcal{A}$ and $\mathcal{B}$ are known matrices and defined by the following equations:

$$
\begin{aligned} \mathcal{A} &= (P^T R^{-1} P)^{-1} P^T R^{-1}, \\ \mathcal{B} &= R^{-1}(I - P\mathcal{A}). \end{aligned} \tag{5}
$$

Hence, we consider cube polynomial $p^T(\mathbf{x}) = [1\, x\, y\, xy\, x^2\, y^2\, xy^2\, yx^2\, x^3\, y^3]$. Moreover:

$$
P = \begin{pmatrix} p_1(\mathbf{x}_1) & \cdots & p_m(\mathbf{x}_1) \\ \cdots & \cdots & \cdots \\ p_1(\mathbf{x}_N) & \cdots & p_m(\mathbf{x}_N) \end{pmatrix}. \tag{6}
$$

The vector $\mathbf{r}(\mathbf{x})$ in Eq. (2) is defined by:

$$
\mathbf{r}^T(\mathbf{x}) = \begin{bmatrix} \gamma(\mathbf{x}, \mathbf{x}_1) & \cdots & \gamma(\mathbf{x}, \mathbf{x}_N) \end{bmatrix}, \tag{7}
$$

where $\gamma(\mathbf{x},\mathbf{x}_j)$ is the correlation function. Many functions may be chosen as a correlation function. In this paper, we choose the following correlation function:

$$\gamma(\mathbf{x},\mathbf{x}_i) = \begin{cases} 1 - 6d_i^2 + 8d_i^3 - 3d_i^4, & d_i \leq 1, \\ 0, & d_i > 1, \end{cases} \tag{8}$$

where $d_i = \dfrac{\|\mathbf{x} - \mathbf{x}_i\|}{r_i}$ and r_i is the size of support in the weight function. Moreover:

$$R = \begin{bmatrix} r(\mathbf{x}_1,\mathbf{x}_1) & \cdots & r(\mathbf{x}_1,\mathbf{x}_N) \\ \cdots & \cdots & \cdots \\ r(\mathbf{x}_N,\mathbf{x}_1) & \cdots & r(\mathbf{x}_N,\mathbf{x}_N) \end{bmatrix}. \tag{9}$$

A MK interpolation shape function $\phi_i(\mathbf{x})$ has the following $\delta - $ Kronecker property:

$$\phi_i(\mathbf{x}_j) = \delta_{ij} = \begin{cases} 1, & i = j, \\ 0, & i \neq 0. \end{cases} \tag{10}$$

To see other essential properties of the MK interpolation shape functions, we refer the readers to [46-48].

3. Numerical Implementation

In this section, we introduce a meshfree technique through the MK scheme for solving Eq. (1).

At first, we generate a fully discrete system of Eq. (1) in the time variable. So, we suppose $\tau = T/n$ as the time step size and $t_k = k\tau, k = 0,1,2,\ldots,n$ are the time discretize points where n is an arbitrary positive integer. Now, to discretization the fractional differential equation (1) in the time variable, we use the following finite difference expressions as [49]:

$$\mathfrak{D}_t^\alpha v(\mathbf{p},t_{n+1}) = c_0 \left[v_{n+1} - 2v_n + v_{n-1} + \sum_{k=1}^n d_k \left(v_{n-k+1} - 2v_{n-k} + v_{n-k-1} \right) \right] + O(\tau^{3-\alpha}),$$
$$\mathfrak{D}_t^\beta v(\mathbf{p},t_{n+1}) = a_0 \left[v_{n+1} - v_n + \sum_{k=1}^n b_k \left(v_{n-k+1} - v_{n-k} \right) \right] + O\left(\tau^{2-\beta}\right), \tag{11}$$

in which $c_0 = \dfrac{\tau^{-\alpha}}{\Gamma(3-\alpha)}, d_k = \left[(k+1)^{2-\alpha} - (k)^{2-\alpha} \right], a_0 = \dfrac{\tau^{-\beta}}{\Gamma(2-\beta)}, b_k = (k+1)^{1-\beta} - (k)^{1-\beta}$ and $v_n = v(\mathbf{p},n\tau)$. Substituting Eq. (11) and the following relation:

$$\mathfrak{D}_t v = \frac{v_{n+1} - v_n}{\tau} + O(\tau), \tag{12}$$

in Eq. (1), results in:

$$c_0 \left[v_{n+1} - 2v_n + v_{n-1} + \sum_{k=1}^n d_k \left(v_{n-k+1} - 2v_{n-k} + v_{n-k-1} \right) \right] + \lambda_1 \frac{v_{n+1} - v_n}{\tau}$$
$$+ \lambda_2 a_0 \left[v_{n+1} - v_n + \sum_{k=1}^n b_k \left(v_{n-k+1} - v_{n-k} \right) \right] + \lambda_3 v_{n+1} = \lambda_4 \Delta v_{n+1} + s(\mathbf{p},t_{n+1}).$$

Simplifying this relation, one obtains the following equation:

$$\begin{aligned} \mu_1 v_{n+1} - \lambda_4 \Delta v_{n+1} \quad &= \mu_2 v_n - c_0 v_{n-1} + s(\mathbf{p},t_{n+1}) \\ &\quad - c_0 \sum_{k=1}^n d_k \left(v_{n-k+1} - 2v_{n-k} + v_{n-k-1} \right) \\ &\quad - \lambda_2 a_0 \sum_{k=1}^n b_k \left(v_{n-k+1} - v_{n-k} \right), \end{aligned} \tag{13}$$

in which $\mu_1 = c_0 + \dfrac{\lambda_1}{\tau} + a_0\lambda_2 + \lambda_3, \mu_2 = 2c_0 + \dfrac{\lambda_1}{\tau} + a_0\lambda_2$. So, the time discretization is completed.

Now, we perform the discretization in space variables by using MK interpolation. For this propose, we assume, $\Omega \subseteq \mathbb{R}^2$ is the global problem domain, and $\mathbf{X}^* = \{\mathbf{p}_1,\mathbf{p}_2,\mathbf{p}_3,\ldots,\mathbf{p}_m\}$ be arbitrary scattered points in the global domain Ω. Also, instead of calculating global weak form, we introduce the weak form over a local subdomain such as $\Omega_\mathbf{p}$, which is a small region environment over each node in the general domain Ω. Moreover, these subdomains can have any desired geometric shapes and sizes [50]. They overlap and cover the entire domain Ω. We assume they are circular in 2D, and for any random point $\mathbf{p} \in \mathbf{X}^*$ we introduce the local weak form of Eq. (1) independent subdomain $\Omega_\mathbf{p} \subset \Omega$ to $\mathbf{p}$. For every point $\mathbf{p}$, the local weak form of Eq. (13) in $\Omega_\mathbf{p}$ is as follows:

$$\begin{aligned} \mu_1 v_{n+1}(\mathbf{p}) - \lambda_4 \Delta v_{n+1}(\mathbf{p}) \quad &= \mu_2 v_n(\mathbf{p}) - c_0 v_{n-1}(\mathbf{p}) + s(\mathbf{p},t_{n+1}) \\ &\quad - c_0 \sum_{k=1}^n d_k \left(v_{n-k+1}(\mathbf{p}) - 2v_{n-k}(\mathbf{p}) + v_{n-k-1}(\mathbf{p}) \right) \\ &\quad - \lambda_2 a_0 \sum_{k=1}^n b_k \left(v_{n-k+1}(\mathbf{p}) - v_{n-k}(\mathbf{p}) \right). \end{aligned} \tag{14}$$

Assuming there are only N points $(N \leq m)$ in the neighborhood of node $\mathbf{p}$ that affect the numerical solution. So, we have:

$$v^h(\mathbf{p},t) = \sum_{j=1}^{N} \phi_j(\mathbf{p}) \hat{v}_j = \Phi(\mathbf{p})\mathbf{v}(t), \quad \mathbf{p} \in \Omega_{\mathbf{p}}. \tag{15}$$

Substituting the MK interpolation Eq. (15) in Eq. (14) the following matrix system for all points will be obtained:

$$\begin{aligned}
\left(\mu_1 \mathcal{C} - \mathcal{K}\right)\mathcal{V}_{n+1} &= \mu_2 \mathcal{C}\mathcal{V}_n - c_0 \mathcal{C}\mathcal{V}_{n-1} + \mathcal{S}_{n+1} \\
&\quad - c_0 \mathcal{C}\sum_{k=1}^{n} d_k \left(\mathcal{V}_{n-k+1} - 2\mathcal{V}_{n-k} + \mathcal{V}_{n-k-1}\right) \\
&\quad - \lambda_2 a_0 \mathcal{C}\sum_{k=1}^{n} b_k \left(\mathcal{V}_{n-k+1} - \mathcal{V}_{n-k}\right).
\end{aligned} \tag{16}$$

Since the shape functions of the MK method have the $\delta - $ Kronecker property, matrix $\mathcal{C}$ is an identical matrix. Also:

$$\mathcal{C}_{Ij} = \phi_j(\mathbf{p}_I) = \begin{cases} 1, & I = j \\ 0, & I \neq j \end{cases}, \qquad \mathcal{K}_{Ij} = \lambda_4 \Delta \phi_j, \qquad \mathcal{S}_{n+1,I} = s(\mathbf{p}_I, (n+1)\tau), \qquad \mathcal{V}_{n,I} = v(\mathbf{p}_I, (n+1)\tau).$$

For $n = 0$, from the initial condition (1) and central finite difference equation, one obtains:

$$\frac{\partial \mathcal{V}(\mathbf{p},0)}{\partial t} = \frac{\mathcal{V}_1 - \mathcal{V}_{-1}}{2\tau} = g(\mathbf{p}) \Rightarrow \mathcal{V}_{-1} = \mathcal{V}_1 - 2\tau G(\mathbf{p}), \tag{17}$$

in which $G(\mathbf{p}) = \left[g(\mathbf{p}_1), \ldots, g(\mathbf{p}_m)\right]^T$.

So, we get:

$$\left((\mu_1 + c_0)\mathcal{C} - \mathcal{K}\right)\mathcal{V}_1 = \mu_2 \mathcal{C}\mathcal{V}_0 + 2c_0 \tau G + \mathcal{S}_1, \tag{18}$$

and for the other n $(n > 0)$, Eq. (16) will be used.

Remark 1: We have done our calculation by using **MATLAB** software on an Intel(R) *Core* (TM) *i7-7700 PC with a 3.60-GHz CPU and 32-GB RAM.*

4. Numerical Examples

In this section, three examples in 2D and one example in 3D are presented to illustrate the capability and validity of our scheme. To show the accuracy of the MLPG method, the L_∞ errors are considered as follows:

$$L_\infty = \max_{1 \leq i \leq N} |v(\mathbf{x}_i) - v^h(\mathbf{x}_i)|, \tag{19}$$

where $v(\mathbf{x}_i)$ and $v^h(\mathbf{x}_i)$ are the exact and numerical solutions at node $\mathbf{x}_i$, respectively.

Moreover, to show the efficiency of the proposed scheme, the following convergence order in the time variable is calculated:

$$c - \text{order} = \frac{\log\left(\frac{L_\infty(\tau_1)}{L_\infty(\tau_2)}\right)}{\log\left(\frac{\tau_1}{\tau_2}\right)},$$

in which $L_\infty(\tau_1)$ and $L_\infty(\tau_2)$ are L_∞ errors related to τ_1 and τ_2, respectively.

Moreover, the global data density of X in regular and irregular domain Ω is as follows [51]:

$$h = h_{\Omega,X} = \sup_{\mathbf{x} \in \Omega} \min_{\mathbf{x}_i \in X} \|\mathbf{x} - \mathbf{x}_i\|.$$

This relation will define subdomains and the size of support in the correlation function for MK interpolation.
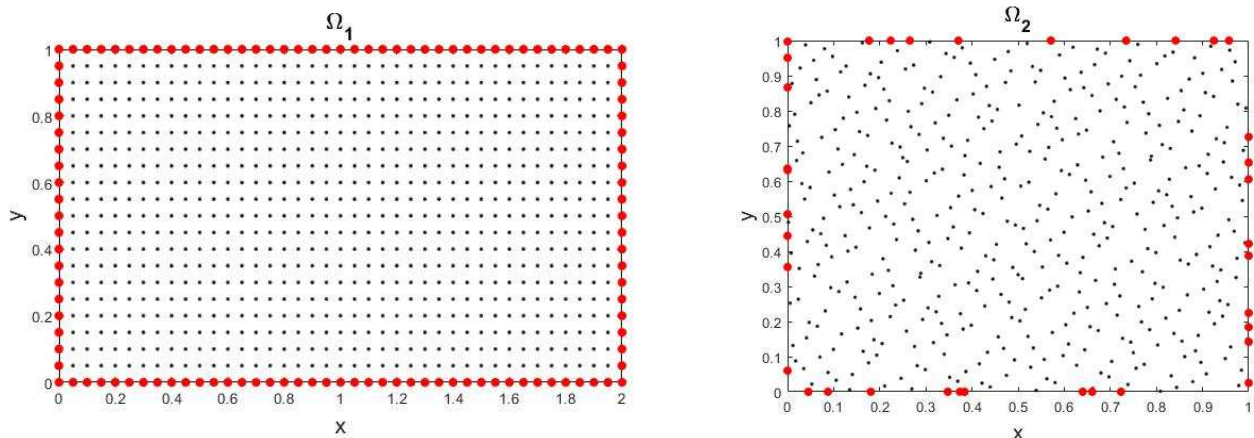

Fig. 3. Rectangular domains with uniform (left) and nonuniformly distributed points (Right) for Example 1.

4.1. Example

In this example, we suppose MHD fractional Maxwell fluid (1) in the following form:

$$\mathfrak{D}_t^\alpha v(\mathbf{p},t) + \mathfrak{D}_t v(\mathbf{p},t) + \mathfrak{D}_t^\beta v(\mathbf{p},t) + v(\mathbf{p},t) = \Delta v(\mathbf{p},t) + s(\mathbf{p},t), \quad (\mathbf{p},t) \in \Omega \times [0,T], \tag{20}$$

with the analytical solution:

$$v(x,y,t) = t^2 x(2-x)y(1-y).$$

Ω_1 in Fig. 3 (left) is assumed as global domain. In this case, the distribution of nodes is regular, the boundary conditions are zero on all sides of Ω_1 and the initial conditions are zero. Also,

$$s(x,y,t) = \left[\frac{2}{\Gamma(3-\alpha)}t^{2-\alpha} + 2t + \frac{2}{\Gamma(3-\beta)}t^{2-\beta}\right]x(2-x)y(1-y) + 2t^2y(1-y) + 2t^2x(2-x) + t^2.$$

To show the accuracy and validity of the proposed scheme, we solve this problem in Ω_1. Hence, the final time is $T = 2$ with the time step size $\tau = 0.001$.

Also, 41×21 regular nodes in Ω_1 are used. Figure 4 shows the absolute error for the presented method and these nodes. In this case, the fractional-order α and β are 1.9 and 0.1, respectively.

Figure 5 shows a comparison between the exact solution and proposed numerical scheme at $y = 0.5$ in Ω_1 with $\alpha = 1.7, \beta = 0.7$.

Table 2 illustrates the results for various fractional orders in different total times $T = 0.5, 1, 3, 5, 7$. From this table, one can see that the proposed method is efficient for this example in large time and different values of fractional orders. These results reveal that the error increases with increasing the final time. The reason is that with increasing the final time, the exact solution increases for example, in $T = 7$, the maximum of the exact solution is $3.9690e + 01$, which is significant.

Table 2 and Fig. 4 demonstrate that our presented scheme is valid and capable of solving this problem. Now, we examine this example in Ω_2 and 441 nonuniform points in this global domain will be used.
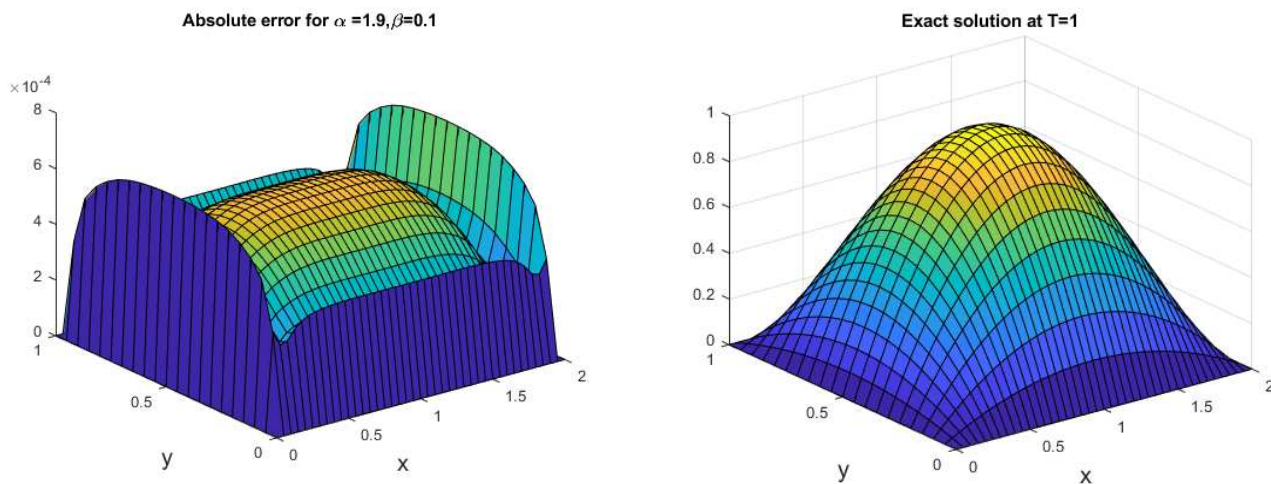

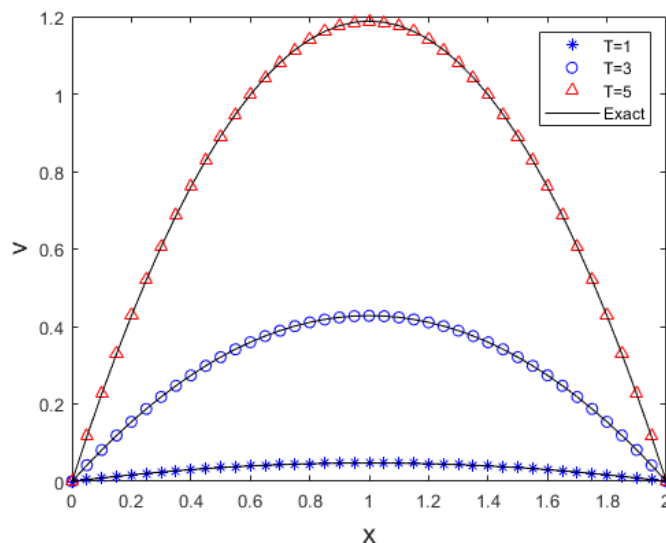**Fig. 4.** The plot of analytical solution and absolute error for Example 1 at $T = 1$.

Fig. 5. Comparison between the analytical solution and proposed scheme at $y = 0.5$, $\alpha = 1.7, \beta = 0.7$ for Example 1.

Table 2. The L_∞ errors of the presented scheme for Example 1 over Ω_1 with different values of final times $T = 0.5, 1$ top to $T = 7$.

T	$\alpha = 1.7, \beta = 0.7$	$\alpha = 1.5, \beta = 0.5$	$\alpha = 1.2, \beta = 0.2$
0.5	$3.7530e-05$	$3.5886e-05$	$3.6909e-05$
1	$1.5149e-04$	$1.5722e-04$	$1.5991e-04$
3	$1.5473e-03$	$1.5464e-03$	$1.5469e-03$
5	$4.8491e-03$	$4.8127e-03$	$4.7778e-03$
7	$1.0216e-02$	$1.0116e-02$	$9.9667e-03$

Table 3. The L_∞ errors of the presented scheme for Example 1 over Ω_2 with $T = 1$ and different step time sizes.

τ	$\alpha = 1.7, \beta = 0.7$	$c-\text{order}$	$\alpha = 1.5, \beta = 0.5$	$c-\text{order}$	$\alpha = 1.3, \beta = 0.3$	$c-\text{order}$
0.01	$3.4952e-04$	$-$	$3.7925e-04$	$-$	$3.6090e-04$	$-$
0.01/2	$1.7185e-04$	1.0242	$1.8564e-04$	1.0306	$1.7652e-04$	1.0318
0.01/4	$8.2675e-05$	1.0556	$8.8993e-05$	1.0607	$8.4459e-05$	1.0635
0.01/8	$3.7839e-05$	1.1276	$4.0736e-05$	1.1274	$3.8464e-05$	1.1347

Table 4. Comparison L_∞ errors of the presented scheme with the obtained results in [37] for Example 1 over Ω_1 at $T = 1$.

dx	dy	τ	Method of [41]	Present method
0.1	0.1	0.01	$2.8213e-03$	$3.8464e-03$
0.5	0.5	0.0025	$6.9283e-04$	$9.5128e-04$
0.025	0.025	0.000625	$1.7161e-04$	$2.3635e-04$

Table 3 demonstrates L_∞ errors for different step times and various fractional orders. Also, the $c-\text{order}$ for this scheme is reported in columns 3, 5 and 7. This table shows that the proposed method has almost $O(\tau)$ convergence order. Also, the time step size is $\tau = 0.01$. Based on the results of Table 3, one observes that the presented method is valid and accurate for irregular distribution points.

To further assess the accuracy of the method, in the next table, we will test different spatial and temporal step sizes at final time. For this purpose, assume Eq. (20) with the following exact solution:

$$v(x, y, t) = t^3 x(2 - x)y(1 - y),$$

we extract the force term $s(x, y, t)$ from this exact solution.

Table 4 illustrates a compression between our scheme and method of [37]. From this table, it can be seen that the proposed method is more accurate than the mentioned method.

4.2. Example

In this example, we suppose the following MHD fractional Maxwell fluid equation:

$$\mathfrak{D}_t^\alpha v(\mathbf{p}, t) + \mathfrak{D}_t v(\mathbf{p}, t) + \mathfrak{D}_t^\beta v(\mathbf{p}, t) + v(\mathbf{p}, t) = \Delta v(\mathbf{p}, t) + s(\mathbf{p}, t), \quad (\mathbf{p}, t) \in \Omega \times [0, T], \tag{21}$$

with the exact solution:

$$v(x, y, t) = t \sin(t) \sin(x) \cos(y).$$

The boundary conditions are:

$$v(x, y, t) = t \sin(t) \sin(x) \cos(y), \qquad (x, y) \in \partial\Omega_3, \partial\Omega_4$$

Also, the initial conditions are zero, and we have,

$$s(x, y, t) = \left[t^2 \sum_{j=0}^{\infty} (2j + 2)t^{2j} \left(\frac{(-1)^j t^{-\alpha}}{\Gamma(2j + 3 - \alpha)} + \frac{(-1)^j t^{-\beta}}{\Gamma(2j + 3 - \beta)} \right) + (1 + 3t)\sin(t) + t\cos(t) \right] \sin(x) \cos(y).$$

We solve this equation on the circular domain by using regular and irregular distribution nodes, as shown in Fig. 6. By using the presented algorithm on the global domain Ω_3 the results are shown in Table 5.

Table 5 indicates the L_∞ errors between our numerical method and the exact solution for this example. We assume the total time is $T = 1$ and $\tau = 0.01$. Also, 126 and 177 nodes are applied on the boundary and interior of Ω_3, respectively. Column one of this table shows the time step sizes which decrease from top to bottom. To test the capability of this scheme, different fractional orders are used (columns 2, 4 and 6). Also, the $c-\text{order}$ is shown in columns 3, 5, and 7. According to the results of this table, the present method has good accuracy compared to the exact solution on the circular domain with regularly distributed nodes. Moreover, this method has almost $O(\tau)$ convergence order.
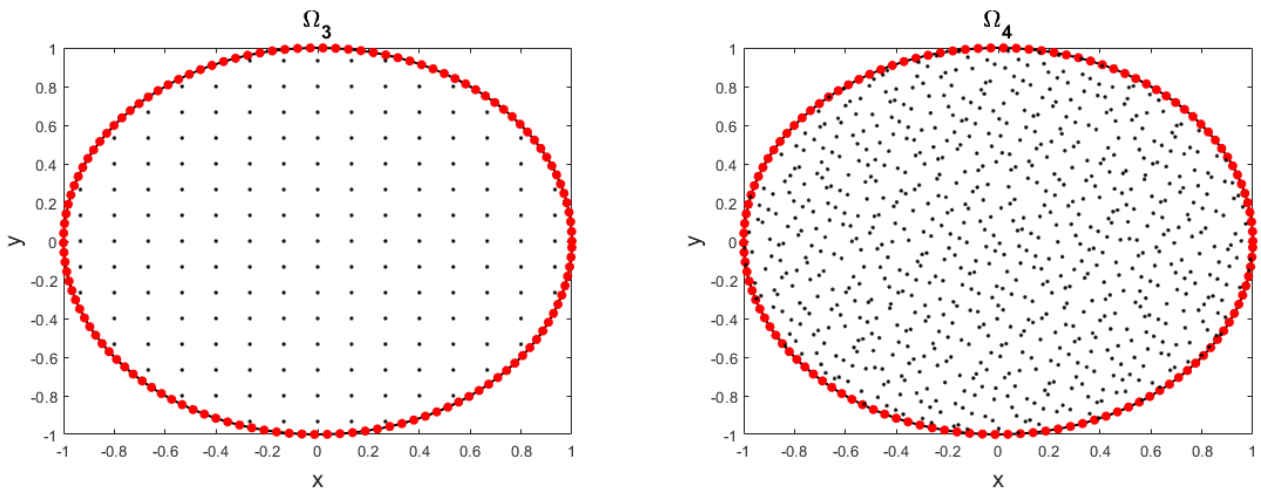
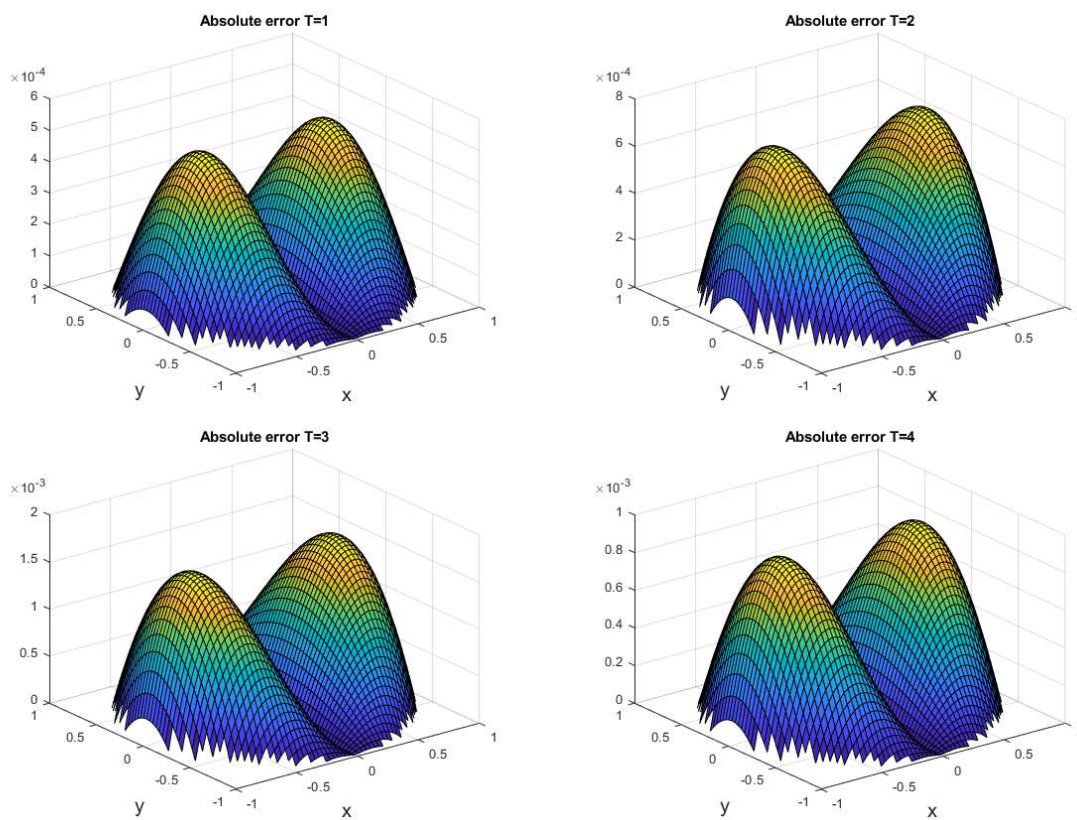**Fig. 6.** Circular domain with regular (Ω_3 left) and irregular distribution of points (Right Ω_4) for Example 2.

Fig. 7. Absolute errors for different final times $T = 1, 2, 3, 4$ with $\tau = 0.01$ for Example 2 in Ω_3.

Table 5. The L_∞ errors of the presented scheme for Example 2 over Ω_4 with $T = 1$ and different step times.

τ	$\alpha = 1.9, \beta = 0.9$	$c - \text{order}$	$\alpha = 1.5, \beta = 0.5$	$c - \text{order}$	$\alpha = 1.2, \beta = 0.2$	$c - \text{order}$
0.01	$1.2872e - 03$	-	$2.8940e - 04$	-	$2.3106e - 04$	-
0.01 / 2	$6.3599e - 04$	1.0172	$1.4801e - 04$	0.9674	$1.2116e - 04$	0.9314
0.01 / 4	$3.1323e - 04$	1.0218	$7.6906e - 05$	0.9445	$6.5329e - 05$	0.8911
0.01 / 8	$1.5461e - 04$	1.0186	$4.2338e - 05$	0.8611	$3.6836e - 05$	0.8266

Table 6. The L_∞ errors of the presented scheme for Example 2 over Ω_4 at different final times.

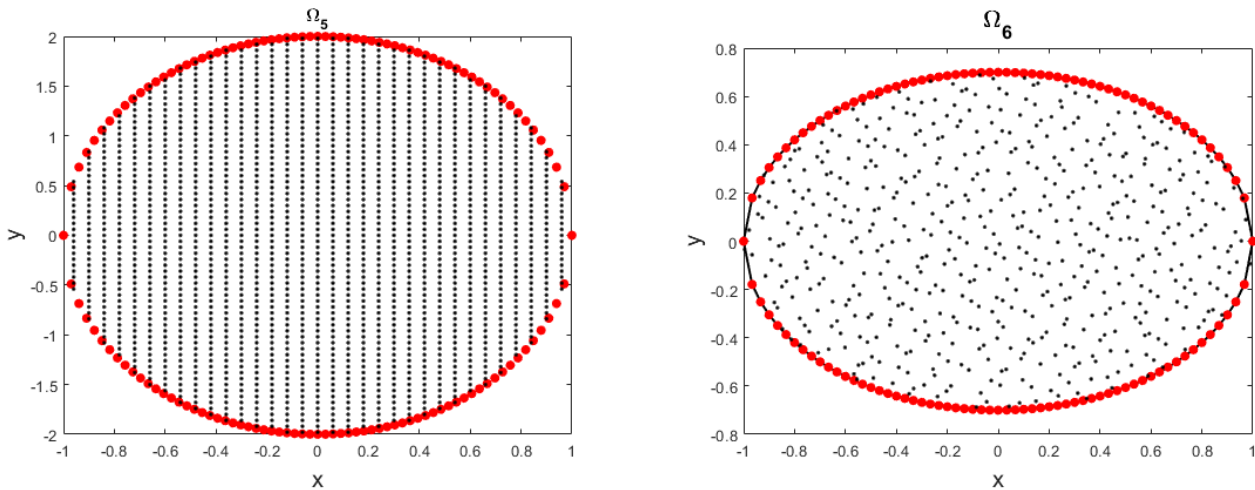| T	$\alpha = 1.7, \beta = 0.7$	$\alpha = 1.5, \beta = 0.5$	$\alpha = 1.2, \beta = 0.2$	time(s)
0.5	$5.4529e - 04$	$1.1961e - 04$	$6.7903e - 05$	2.9
1	$4.7609e - 04$	$2.7378e - 04$	$2.1691e - 04$	3.1
3	$1.7629e - 03$	$1.5377e - 03$	$1.0030e - 03$	4.1
5	$1.8673e - 03$	$1.5384e - 03$	$8.8930e - 04$	5.5
7	$3.0999e - 03$	$2.9802e - 03$	$2.4303e - 03$	7.5

Fig. 8. Elliptical domains with regular (Ω_5 left) and irregular distributed nodes (Right Ω_6) for Example 3.

Figure 7 demonstrates absolute errors at different final times for $\alpha = 1.7, \beta = 0.7$. This figure shows that this method is accurate for a long time.

Table 6 illustrates L_∞ errors for this example in the global domain Ω_4 for different values of fractional orders at various final times. The number of points in the boundary of Ω_4 is 126, and 756 irregular nodes in the interior domain Ω_4 are selected while the time step size is $\tau = 0.01$. Note that the arrangement of nodal points is not regular. So, this scheme is efficient in nonuniformly distributed nodes for a circular domain. The last column of this table is CPU time while running the proposed scheme. The obtained results in Table 6 and Fig. 7 reveal that the presented method has good accuracy for the numerical solution of this example.

4.3. Example

Similar to the previous examples, we examine the capability of our scheme in two global elliptical domains Ω_5 and Ω_6. Let the following governing equation of unsteady 2D flow of a MHD fractional Maxwell fluid equation:

$$\mathfrak{D}_t^\alpha v(\mathbf{p},t) + \mathfrak{D}_t v(\mathbf{p},t) - \mathfrak{D}_t^\beta v(\mathbf{p},t) + v(\mathbf{p},t) = 2\Delta v(\mathbf{p},t) + s(\mathbf{p},t), \quad (\mathbf{p},t) \in \Omega \times [0,T], \qquad (22)$$

subject to the initial conditions:

$$v(x,y,0) = v_t(x,y,0) = 0.$$

The exact solution is:

$$v(x,y,t) = t^2 e^{x+y+t},$$

while the function s is as follows:

$$s(x,y,t) = \left[\sum_{j=0}^{\infty} \frac{(j+1)(j+2)}{\Gamma(j+3-\alpha)} t^{j+2-\alpha} + 2te^t - \sum_{j=0}^{\infty} \frac{(j+1)(j+2)}{\Gamma(j+3-\beta)} t^{j+2-\beta} - 2t^2 e^t \right] \times e^{x+y}.$$

The global domains for this example are shown in Fig. 8. We assume the boundary conditions as Dirichlet type and are derived from the exact solution.

Table 7 indicates the L_∞ errors between the exact solution and our scheme for several fractional orders on the global domain Ω_5. This domain has the following form:

$$x^2 + \frac{1}{4} y^2 = 1.$$

We applied 400 and 1755 nodes in the boundary and interior of Ω_5, respectively. Also, the final time is $T = 1$. According to the results of this table, one observes that, with decreasing the time step size, the error is reduced and the method has almost $O(\tau)$ order of convergence.

Figure 9 shows the results of the exact solution and absolute error for $T = 1$ with $\alpha = 1.7, \beta = 0.7$. Also, the scatter of points the Ω_5 is regular. To test the accuracy of the proposed method in irregularly scattering nodes, the discussion is continued on the domain Ω_6.

Table 7. The L_∞ errors of the presented scheme for Example 3 over Ω_6 with $T = 1$ and different step times.

τ	$\alpha = 1.7, \beta = 0.7$	$c - \text{order}$	$\alpha = 1.5, \beta = 0.5$	$c - \text{order}$	$\alpha = 1.3, \beta = 0.3$	$c - \text{order}$
0.001	$4.4085e-03$	-	$1.1195e-03$	-	$1.3524e-03$	-
0.001 / 2	$2.1259e-03$	1.0522	$5.3152e-04$	1.0747	$6.9147e-04$	0.9678
0.001 / 4	$1.0308e-03$	1.0443	$2.5488e-04$	1.0603	$3.5242e-04$	0.9724
0.001 / 8	$5.0285e-04$	1.0356	$1.2254e-04$	1.0566	$1.8049e-04$	0.9655

Table 8 demonstrates the results in Ω_6, which has the following form:

$$x^2 + \frac{100}{49} y^2 = 1.$$

We applied 200 and 528 points in the boundary and interior of Ω_6, respectively. The first column of Table 8 shows different final times, and other columns report L_∞ errors for various values of fractional orders. The last column is CPU time. The results of this table show that our method has good accuracy in irregular scattering points and large final times.

Figure 10 illustrates the absolute errors for the proposed method at different values of fractional orders at $T = 1$ with $\tau = 0.001$ over Ω_6.

Also, in this example, elliptical domains with regular and irregular scattering nodes were discussed. Due to the results and figures given for domains Ω_5 and Ω_6, it can be concluded that the method has good performance for the numerical solution of this example.
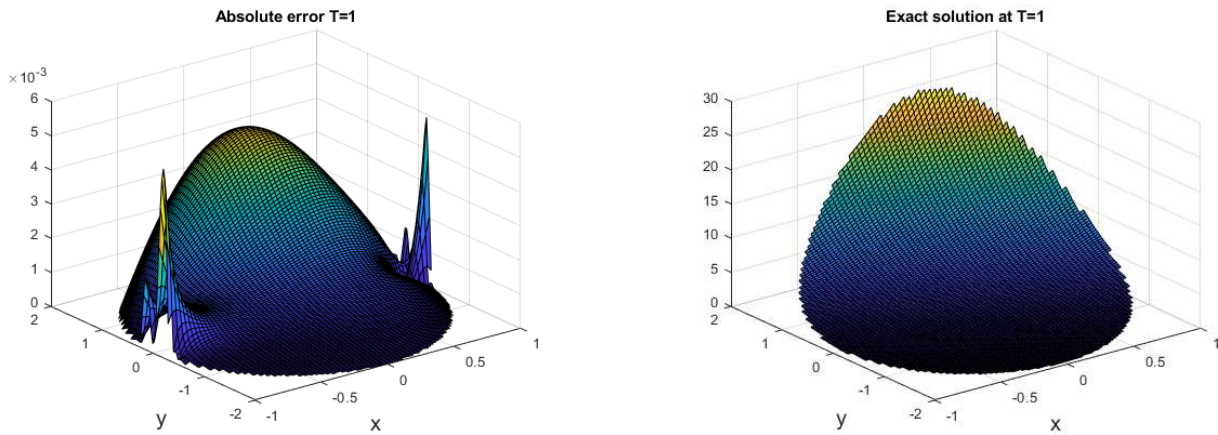
Fig. 9. The plot of analytical solution and absolute error at $T = 1$ for Example 3.
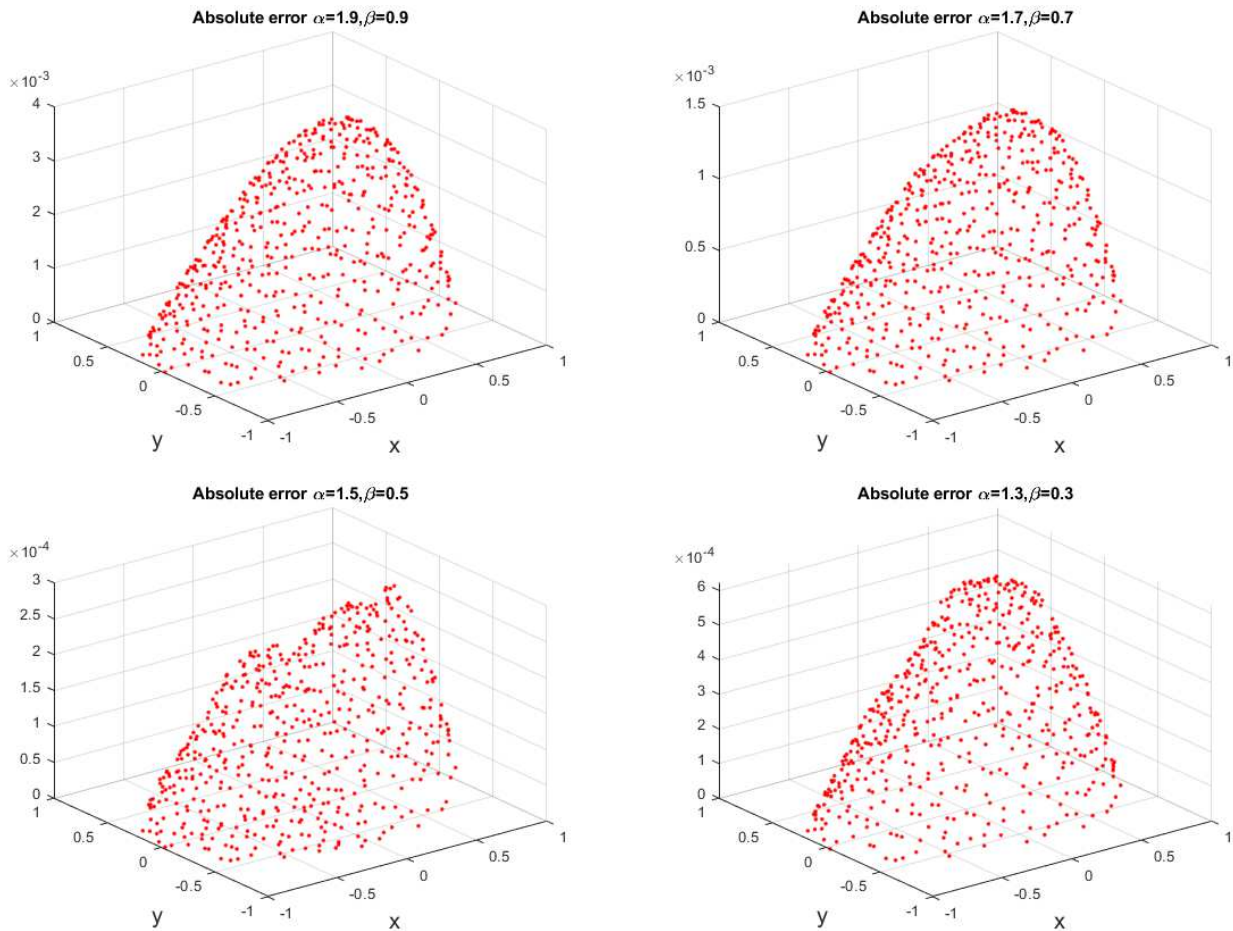

Fig. 10. Absolute errors for the proposed method in different values fractional orders at $T = 1$ with $\tau = 0.001$ for Example 3 in Ω_6.

Table 8. The L_∞ errors of the presented scheme for Example 3 over Ω_7 at different final times.

T	$\alpha = 1.8, \beta = 0.8$	$\alpha = 1.5, \beta = 0.5$	$\alpha = 1.3, \beta = 0.3$	CPU-time
0.5	$5.0490e - 04$	$7.6339e - 05$	$1.9721e - 04$	3.5
1	$2.2424e - 03$	$2.8360e - 04$	$6.2188e - 04$	5.0
3	$4.0877e - 02$	$6.7875e - 03$	$2.7245e - 02$	6.0
5	$5.2255e - 01$	$1.6533e - 01$	$5.1132e - 01$	7.5
7	$5.8337e + 00$	$2.7275e + 00$	$7.0554e + 00$	9.0

Table 9. The L_∞ errors of the presented scheme for Example 4 over Ω_7 with $T = 0.5$ and different step times.

τ	$\alpha = 0.85$	$c - order$	$\alpha = 0.75$	$c - order$	$\alpha = 0.65$	$c - order$
0.001	$4.4085e - 03$	-	$9.6981e - 05$	-	$1.3934e - 04$	-
0.001 / 2	$2.2170e - 04$	1.2113	$3.8535e - 05$	1.3315	$5.7989e - 05$	1.2648
0.001 / 4	$9.5617e - 05$	1.2693	$1.8959e - 04$	1.0233	$2.1362e - 05$	1.4407

Table 10. The L_∞ errors of the presented scheme for Example 4 over Ω_8 with $T = 0.5$ and different step times.

τ	$\alpha = 0.95$	$c - order$	$\alpha = 0.75$	$c - order$	$\alpha = 0.65$	$c - order$
0.01	$4.9386e - 04$	-	$1.9024e - 04$	-	$4.6256e - 05$	-
0.01 / 2	$2.5305e - 04$	0.9647	$8.6197e - 05$	1.1421	$2.7820e - 05$	0.7335
0.01 / 4	$1.2631e - 04$	1.0025	$3.9531e - 05$	1.1247	$1.5101e - 05$	0.8815

4.4. Example

In the last example, consider the fractional telegraph equation with the following form:

$$\mathfrak{D}_t^{2\alpha} v(\mathbf{p}, t) + \mathfrak{D}_t^\alpha v(\mathbf{p}, t) + v(\mathbf{p}, t) = \Delta v(\mathbf{p}, t) + s(\mathbf{p}, t), \quad (\mathbf{p}, t) \in \Omega \times [0, T], \tag{23}$$

where, $\Omega \subseteq \mathbb{R}^3, \Delta = \dfrac{\partial^2}{\partial x^2} + \dfrac{\partial^2}{\partial y^2} + \dfrac{\partial^2}{\partial z^2}$ and the exact solution is $v(x, y, z, t) = t^2 e^{-(x+y+z+t)}$.

Also, the initial conditions are:

$$v(x, y, z, 0) = 0, \qquad v_t(x, y, z, 0) = 0, \qquad (x, y, z) \in \Omega_7$$

and

$$s(x, y, z, t) = [\sum_{j=0}^{\infty} \frac{(-1)^j (j+2)(j+1)}{\Gamma(j+3-2\alpha)} t^{j+2-2\alpha} + \sum_{j=0}^{\infty} \frac{(-1)^j (j+2)(j+1)}{\Gamma(j+3-\alpha)} t^{j+2-\alpha} - 2t^2 e^{-t}] e^{-(x+y+z)}.$$

The boundary conditions are chosen Dirichlet and will be determined from the exact solution. To solve this problem in 3D, 872 points on the sphere shell (blue nodes) and 459 points inside the sphere (red nodes) are used (see Fig. 11). Table 9 reports the results of our meshless scheme compared with the analytical solution for several fractional orders of the 3D fractional telegraph equation. Also, the final time is $T = 0.5$. Due to the results of this table, one can be concluded that the present technique can obtain a suitable numerical solution for this example on a spherical domain.

In the global domain Ω_8, $11 \times 11 \times 11$ uniform nodes are used to solve Eq. (23) by our scheme. Table 10 demonstrates L_∞ errors for different step times and various fractional orders. Also, the convergence orders of this scheme are reported in columns 3, 5, and 7. This table shows that the proposed method has almost $O(\tau)$. Table 11 indicates the results for the 3D case with the final times 1, 2, 3, and 4, and time step $\tau = 0.01$. These calculations were done for different fractional orders, and the results show that our scheme is accurate for this example in the large final times.
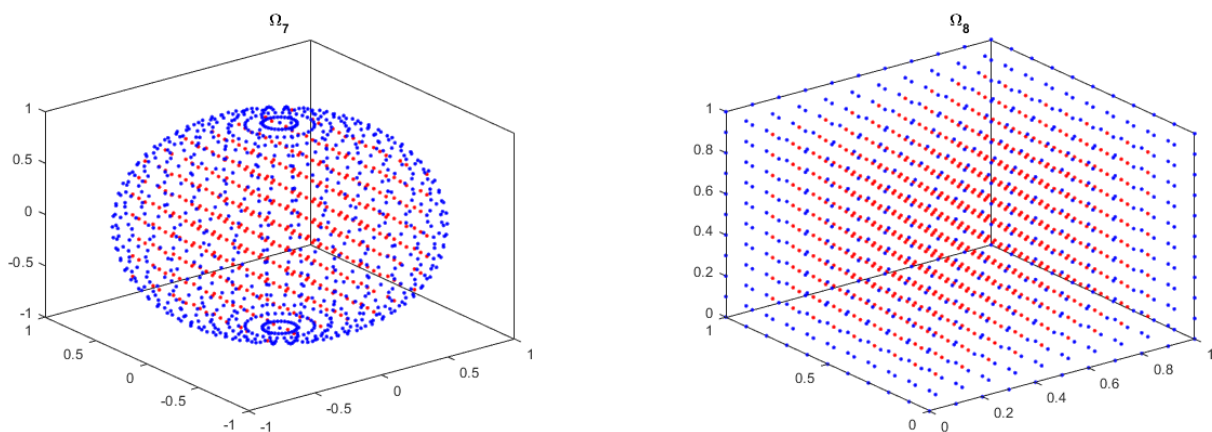

Fig. 11. A sphere (Ω_7) with center (0,0,0) and a cube for 3D problem domain in Example 4.

Table 11. The L_∞ errors of the presented scheme for Example 4 over Ω_8 in different final times.

T	$\alpha = 0.95$	$\alpha = 0.8$	$\alpha = 0.65$
1	$3.8787e-04$	$8.1082e-05$	$5.1166e-05$
2	$2.3965e-04$	$5.2939e-05$	$4.4134e-05$
3	$5.3146e-03$	$3.9878e-03$	$3.0209e-03$
4	$1.4383e-01$	$1.0628e-01$	$9.0918e-02$

Moreover, to show the efficiency of the proposed method in the 3D case, results are obtained on several planes of the cube. Figure 12 demonstrates the absolute errors between our proposed technique and the exact solution for several plates $(x = 0.5, x = 0.9, y = 0.5, y = 0.9, z = 0.5, z = 0.9)$ with the final time $T = 1$ and time step $\tau = 0.01$. This Figure and Tables 9, 10 and 11 show the capability of our scheme for the three-dimensional mode.
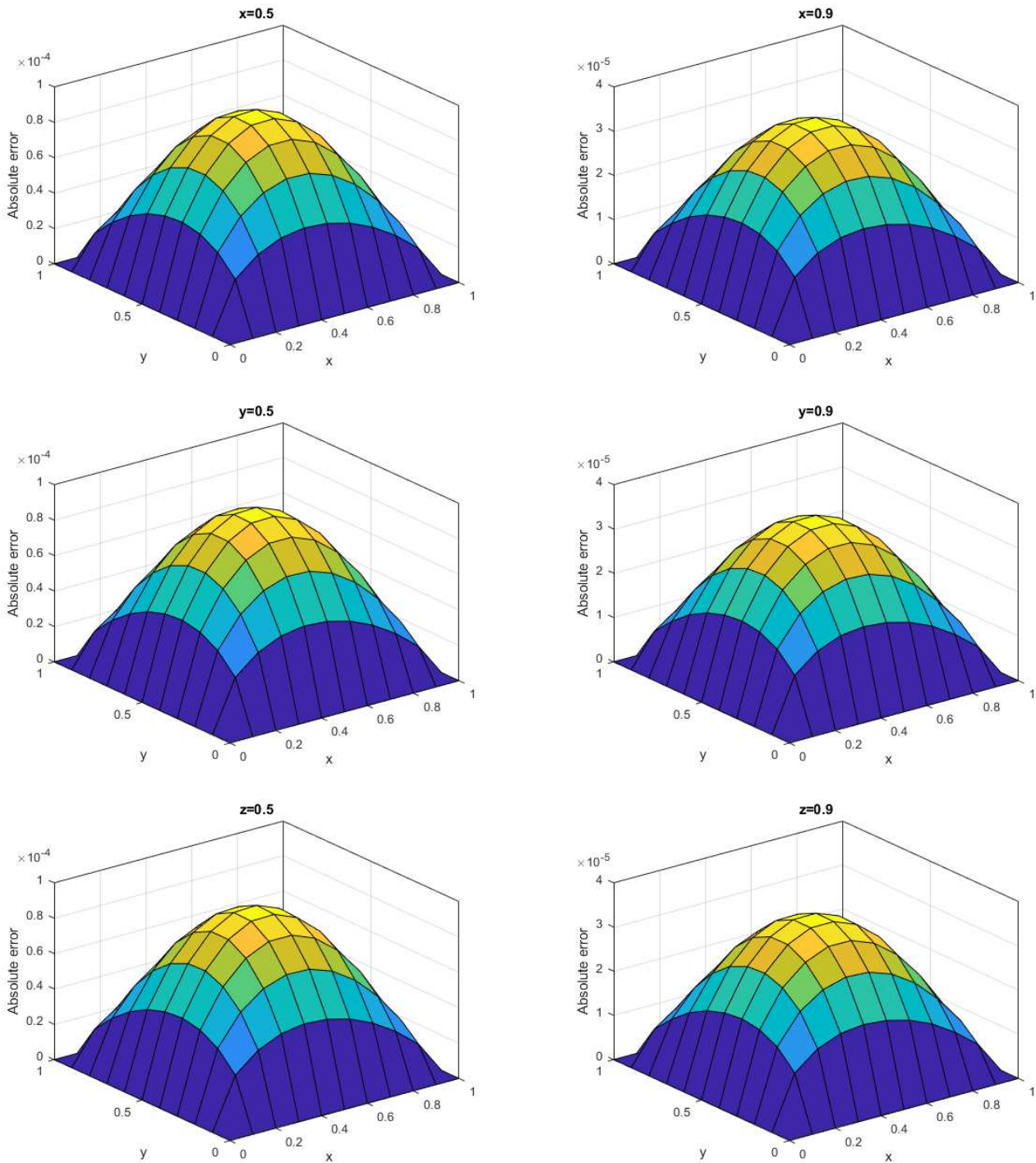
Fig. 12. Absolute errors in different plots at $T = 1$ with $\tau = 0.01, \alpha = 0.85$ in the 3D for Example 4.

5. Conclusion

The Magnetohydrodynamic Maxwell fluid model is an important fractional partial differential equation. In this work, an efficient mesh-free method was used for its numerical solution. In this technique, we applied the moving Kriging interpolation method to create the shape functions of the MLPG method. Since the MK interpolation shape functions have Kronecker's delta property, the boundary conditions could be imposed easily. Also, to approximate the time-fractional derivative, the finite difference relations were be used. The validity and efficiency of this scheme were illustrated by solving three examples in 2D and one example in 3D. The obtained results showed the ability of our method for the numerical solution of fractional MHD flow of viscoelastic fluids and fractional telegraph equation.

Author Contributions

A. Habibrad: Programming and writing draft of the paper, E. Hesameddini and M.H. Heydari: Supervision of the project and revising of the draft, Y. Shekari: Conceptualization, writing and revising of the paper, O. Baghani: Software and revising of the draft. The manuscript was written through the contribution of all authors. All authors discussed the results, reviewed, and approved the final version of the manuscript.

Acknowledgments

Not Applicable.

Conflict of Interest

The authors declared that they have no conflict of interest.

Funding

The authors received no financial support for the research, authorship, and publication of this article.

Data Availability Statements

No datasets are associated with this manuscript.

References

[1] Miller, K.S., Ross, B., *An introduction to the fractional calculus and fractional differential equations*, Wiley, 1993.

[2] Kilbas, A.A., Srivastava, H.M., Trujillo, J.J., *Theory and applications of fractional differential equations*, Elsevier, 2006.

[3] Magin, R.L., Fractional calculus models of complex dynamics in biological tissues, *Computers & Mathematics with Applications*, 59(5), 2010, 1586-1593.

[4] Metzler, R., Klafter, J., The restaurant at the end of the random walk: recent developments in the description of anomalous transport by fractional dynamics, *Journal of Physics A: Mathematical and General*, 37(31), 2004, R161.

[5] Bagley, R.L., Torvik, P.J., A theoretical basis for the application of fractional calculus to viscoelasticity, *Journal of Rheology*, 27(3), 1983, 201-210.

[6] Dehghan, M., Abbaszadeh, M., An efficient technique based on finite difference/finite element method for solution of two-dimensional space/multi-time fractional Bloch-Torrey equations, *Applied Numerical Mathematics*, 131, 2018, 190-206.

[7] Dehghan, M., Safarpoor, M., Abbaszadeh, M., Two high-order numerical algorithms for solving the multi-term time fractional diffusion-wave equations, *Journal of Computational and Applied Mathematics*, 290, 2015, 174-195.

[8] Jin, B., Lazarov, R., Liu, Y., Zhou, Z., The Galerkin finite element method for a multi-term time-fractional diffusion equation, *Journal of Computational Physics*, 281, 2015, 825-843.

[9] Li, Ch., Wang, Zh., The local discontinuous Galerkin finite element methods for Caputo-type partial differential equations: Numerical analysis, *Applied Numerical Mathematics*, 140, 2019, 1-22.

[10] Liu, Q., Liu, F., Turner, I., Anh, V., Finite element approximation for a modified anomalous sub-diffusion equation, *Applied Mathematical Modelling*, 35(8), 2011, 4103-4116.

[11] Biswal, U., Chakraverty, S., Investigation of Jeffery-Hamel flow for nanofluid in the presence of magnetic field by a new approach in the optimal homotopy analysis method, *Journal of Applied and Computational Mechanics*, 8(1), 2022, 48-59.

[12] Pandey, P., Kumar, S., Gómez-Aguilar, J.F., Numerical solution of the time fractional reaction-advection-diffusion equation in porous media, *Journal of Applied and Computational Mechanics*, 8(1), 2022, 84-96.

[13] Ahmad, H., Khan, T.A., Variational iteration algorithm-i with an auxiliary parameter for wave-like vibration equations, *Journal of Low Frequency Noise, Vibration and Active Control*, 38(3-4), 2019, 1113-1124.

[14] Ahmad, H., Variational iteration method with an auxiliary parameter for solving differential equations of the fifth order, *Nonlinear Science Letters A*, 9(1), 2018, 27-35.

[15] Inc, M., Khan, H., Baleanu, D., Khan, A., Modified variational iteration method for straight fins with temperature dependent thermal conductivity, *Thermal Science*, 22(Suppl. 1), 2018, 229-236.

[16] Baseri, A., Abbasbandy, S., Babolian, E., A collocation method for fractional diffusion equation in a long time with Chebyshev functions, *Applied Mathematics and Computation*, 322, 2018, 55-65.

[17] Esen, A., Tasbozan, O., Ucar, Y., Yagmurlu, N.M., A B-spline collocation method for solving fractional diffusion and fractional diffusion-wave equations, *Tbilisi Mathematical Journal*, 8(2), 2015, 181-193.

[18] Hidayat, M.I.P., Ariwahjoedi, B., Parman, S., B-spline collocation method for boundary value problems in complex domains, *International Journal of Computing Science and Mathematics*, 7(2), 2016, 110-125.

[19] Nagy, A.M., Numerical solution of time fractional nonlinear Klein-Gordon equation using Sinc-Chebyshev collocation method, *Applied Mathematics and Computation*, 310, 2017, 139-148.

[20] Pirkhedri, A., Javadi, H.H.S., Solving the time-fractional diffusion equation via Sinc-Haar collocation method, *Applied Mathematics and Computation*, 257, 2015, 317-326.

[21] Kwak, S., Kim, K., An, K., Jong, G., Yun, J., A novel meshfree method for three-dimensional natural frequency analysis of thick laminated conical, cylindrical shells and annular plates, *Physica Scripta*, 96(12), 2021, 125204.

[22] Dehghan, M., Abbaszadeh, M., Mohebbi, A., An implicit RBF meshless approach for solving the time fractional nonlinear Sine-Gordon and Klein-Gordon equations, *Engineering Analysis with Boundary Elements*, 50, 2015, 412-434.

[23] Salehi, R., A meshless point collocation method for 2-D multi-term time fractional diffusion-wave equation, *Numerical Algorithms*, 74(4), 2017, 1145-1168.

[24] Shivanian, E., A new spectral meshless radial point interpolation (SMRPI) method: a well-behaved alternative to the meshless weak forms, *Engineering Analysis with Boundary Elements*, 54, 2015, 1-12.

[25] Shokri, A., Habibirad, A., A moving Kriging-based MLPG method for nonlinear Klein-Gordon equation, *Mathematical Methods in the Applied Sciences*, 39(18), 2016, 5381-5394.

[26] Habibirad, A., Hesameddini, E., Taleei, A., An efficient meshless method for solving multi-dimensional nonlinear Schrödinger equation, *Iranian Journal of Science and Technology, Transactions A: Science*, 44(3), 2020, 749-761.

[27] Habibirad, A., Hesameddini, E., Heydari, M.H., Roohi, R., An efficient meshless method based on the moving kriging interpolation for two-dimensional variable-order time fractional Mobile/Immobile advection-diffusion model, *Mathematical Methods in the Applied Sciences*, 44(4), 2021, 3182-3194.

[28] Bui, B., Saasen, A., Maxey, J., Ozbayoglu, M.E., Miska, S.Z., Yu, M., Takach, N.E., Viscoelastic properties of oil-based drilling fluids, *Annual Transactions of the Nordic Rheology Society*, 20, 2012, 33-47.

[29] Makarynska, D., Gurevich, B., Behura, J., Batzle, M., Fluid substitution in rocks saturated with viscoelastic fluids, *Geophysics*, 75(2), 2010, 115-122.

[30] Khan, Z., Rasheed, H.U., Islam, S., Noor, S., Khan, I., Abbas, T., Khan, W., Seikh, A.H., Sherif, E.S.M., Nisar, K.S., Heat transfer effect on viscoelastic fluid used as a coating material for wire with variable viscosity, *Coatings*, 10(2), 2020, 163.

[31] Kumar, N.N., Praveen, B.V.S., Pulsatile Oldroyd-b blood flow dynamics in a stenosed artery, *International Journal of Advances in Engineering Sciences and Applied Mathematics*, 12, 2020, 233–241.

[32] Pérez-Reyes, I., Vargas-Aguilar, R.O., Pérez-Vega, S.B., Ortiz-Pérez, A.S., *Applications of viscoelastic fluids involving hydrodynamic stability and heat transfer*, Polymer Rheology, IntechOpen, 2018, DOI: 10.5772/intechopen.76122.

[33] Chhabra R.P., Richardson, J.F., *Non-Newtonian flow and applied rheology: engineering applications*, Butterworth-Heinemann, 2011.

[34] Bruce, S.A., Nonlinear Maxwell equations and strong-field electrodynamics, *Physica Scripta*, 97(3), 2022, 035303.

[35] Wenchang, T., Wenxiao, P., Mingyu, X., A note on unsteady flows of a viscoelastic fluid with the fractional Maxwell model between two parallel plates, *International Journal of Non-Linear Mechanics*, 38(5), 2003, 645-650.

[36] Hossain M.E., Islam, M.R., Fluid properties with memory--a critical review and some additions, *In Proc. 36th International Conference on Computers and Industrial Engineering*, CIE-00778, Taipei, Taiwan, 20-23, 2006.

[37] Zhang, Y., Zhao, H., Liu, F., Bai, Y., Analytical and numerical solutions of the unsteady 2D flow of MHD fractional Maxwell fluid induced by variable pressure gradient, *Computers & Mathematics with Applications*, 75(3), 2018, 965-980.

[38] Chen, X., Yang, W., Zhang, X., Liu, F., Unsteady boundary layer flow of viscoelastic MHD fluid with a double fractional Maxwell model, *Applied Mathematics Letters*, 95, 2019, 143-149.

[39] Chen, X., Ye, Y., Zhang, X., Zheng, L., Lie-group similarity solution and analysis for fractional viscoelastic MHD fluid over a stretching sheet, *Computers & Mathematics with Applications*, 75(8), 2018, 3002-3011.

[40] Feng, L., Liu, F., Turner, I., Zheng, L., Novel numerical analysis of multi-term time fractional viscoelastic non-Newtonian fluid models for simulating unsteady MHD Couette flow of a generalized Oldroyd-b fluid, *Fractional Calculus and Applied Analysis*, 21(4), 2018, 1073-1103.

[41] Moustafa, E.S., MHD of a fractional viscoelastic fluid in a circular tube, *Mechanics Research Communications*, 33(2) 2006, 261-268.

[42] Sheikholeslami, M., New computational approach for exergy and entropy analysis of nanofluid under the impact of Lorentz force through a porous media, *Computer Methods in Applied Mechanics and Engineering*, 344, 2019, 319-333.

[43] Sheikholeslami, M., Numerical approach for MHD Al2O3-Water nanofluid transportation inside a permeable medium using innovative computer method, *Computer Methods in Applied Mechanics and Engineering*, 344, 2019, 306-318.

[44] Sheikholeslami, M., Ellahi, R., Three-dimensional mesoscopic simulation of magnetic field effect on natural convection of nanofluid, *International Journal of Heat and Mass Transfer*, 89, 2015, 799-808.

[45] Kwak, S., Kim, K., An, K., Kim, N., Kim, H., A meshfree moving least squares-T-Chebyshev shape function approach for free vibration analysis of laminated composite arbitrary quadrilateral plates with hole, *Physica Scripta*, 96(7), 2021, 075216.

[46] Chen, L., Liew, K.M., A local Petrov-Galerkin approach with moving kriging interpolation for solving transient heat conduction problems, *Computational Mechanics*, 47, 2011, 455-467.

[47] Gu, L., Moving Kriging interpolation and element-free Galerkin method, *International Journal for Numerical Methods in Engineering*, 56, 2003, 1-11.

[48] Liang, Q., Dai, B., Zheng B., Wang, L., Numerical solution of transient heat conduction problems using improved meshless local Petrov-Galerkin method, *Applied Mathematics and Computation*, 219, 2013, 10044-10052.

[49] Shivanian, E., Spectral meshless radial point interpolation (SMRPI) method to two-dimensional fractional Telegraph equation, *Mathematical Methods in the Applied Sciences*, 39(7), 2016, 1820-1835.

[50] Atluri, S.N., Zhu, T., A new meshless local Petrov-Galerkin (MLPG) approach in computational mechanics, *Computational Mechanics*, 22(2), 1998, 117-127.

[51] Wang, T., Zhang, L., Wu, H., Zhang, X., Jin, Y., Yang, P., Xu, C., Effect of Mold Electromagnetic Stirring on the Flow and Solidification of Φ 800 mm Round Blooms, *Processes*, 10(2), 2022, 430.

[52] Fasshauer, G.E., *Meshfree approximation methods with MATLAB*, World Scientific, 2007.

ORCID ID

Ali Habibirad⬤ https://orcid.org/0000-0002-7701-1467

Esmail Hesameddini⬤ https://orcid.org/0000-0002-7012-1161

Younes Shekari⬤ https://orcid.org/ 0000-0003-2357-1773

Mohammad Hossein Heydari⬤ https://orcid.org/0000-0002-2169-9485

Omid Baghani⬤ https://orcid.org/0000-0002-5429-9373

Publisher's Note Shahid Chamran University of Ahvaz remains neutral with regard to jurisdictional claims in published maps and institutional affiliations.